Optics and Lasers in Engineering 47 (2009) 1056–1062

Contents lists available at ScienceDirect

Optics and Lasers in Engineering

journal homepage: www.elsevier.com/locate/optlaseng

# Fiber optic acoustic emission sensor and its applications in the structural health monitoring of CFRP materials

Tao Fu [a], Yanju Liu [b], Quanlong Li [c], Jinsong Leng [a,*]

[a] Centre for Composite Materials, No. 2 YiKuang Street, P.O. Box 3011, Science Park of Harbin Institute of Technology, Harbin 150080, PR China
[b] Department of Aerospace Science and Mechanics, No. 92 West DaZhi Street, Harbin Institute of Technology (HIT), Harbin 150001, PR China
[c] Department of Computer Science and Engineering, No. 92 West DaZhi Street, Harbin Institute of Technology (HIT), Harbin 150001, PR China

ARTICLE INFO

Available online 14 July 2009

*Keywords:*
Fiber optic sensor
Acoustic emission (AE)
Composite structures
Structural health monitoring (SHM)
CFRP materials

ABSTRACT

A fiber optic acoustic emission sensor based on fused-tapered coupler and its applications in structural health monitoring are proposed in this paper. The fiber optic acoustic emission sensor (FOAES) was tested using pencil lead break tests compared with the commercial acoustic emission sensor (R15 PZT). Besides, the sensor was embedded into the carbon fiber reinforced plastics (CFRP) materials and tested in the same way. It successfully detected the AE signals. FOAES was applied in the structural health monitoring (SHM) of CFRP materials. Damages of carbon fiber/epoxy composite laminates during three-point-bending test were monitored by surface-mounted and embedded FOAES, respectively. Results identified that the sensor embedded into composite structures could monitor damage of composite laminates on-line as the surface-mounted sensor did.



## 1. Introduction

Acoustic emission is a class of phenomena whereby transient elastic waves are generated by the rapid release of energy from a localized source or sources within a material. Typically, the transient elastic waves are detected by commercial acoustic emission sensors that are usually of piezoelectric type. However, these electrically powered sensors have disadvantages that preclude their deployment in particular circumstances. For example, they are sensitive to electromagnetic interference or radio frequency and hence are out of work in environments with a high electrical potential. Compared with it, fiber optic sensors have the following attractive features: (i) their material properties are similar to reinforcing fibers of composite materials; (ii) they can be easily embedded in arbitrary shapes using their small, flexible and lightweight natures; (iii) they are immune to electromagnetic interference due to their dielectric nature; (iv) they have increased sensitivity and can measure many physical quantities simultaneously at many points.

Even though a mass of multiform fiber optic sensors have been applied to measure strain, temperature [1–3] and vibration [4] for structural health monitoring (SHM), they cannot monitor materials damage availably as AE sensors. The majority of the fiber optic acoustic emission sensors (FOAES) reported to date in the literature are based on one of the following techniques: (i) Mach–Zehnder interferometer [5], (ii) Michelson interferometer, (iii) Fabry–Perot interferometer [6,7], (iv) Sagnac interferometer [8], (v) EFPI and FBG sensors [9], and (vi) a strain-free FBG sensor [10]. However, those sensing techniques have the drawbacks of being relatively expensive, complicated to implement on-site.

A fiber optic acoustic emission sensor based on a fused-tapered fiber coupler has been investigated [11–13]. However, their fiber optic sensor is packaged with V-grooved substrates and is not compatible to embed in composite materials. Leng et al. have recently reported a multi-functional fiber optic sensor which could identify types of failures of composite materials and measure temperature and strain at the same time [14]. In this paper, we fabricated fiber optic acoustic emission sensors as a structural health monitoring device, consisting of silica capillary tube and fused-tapered fiber. And then the sensor calibration experiments were carried out, including the calibration experiment of FOAES attached to the surface of specimen and the calibration experiment of FOAES embedded in CFRP laminates. Finally, the CFRP laminates surface-mounted with FOAES and that embedded with FOAES were tested to monitor their damages during three-point bending tests.

## 2. FOAES and its calibration tests

### 2.1. FOAES

The basic schematic illustration of the acoustic emission (AE) sensor used for structural health monitoring is shown in Figs. 1

* Corresponding author. Tel./fax: +86 451 8640 2328.
*E-mail address:* lengjs@hit.edu.cn (J. Leng).

0143-8166/$ - see front matter © 2009 Elsevier Ltd. All rights reserved.
doi:10.1016/j.optlaseng.2009.03.011

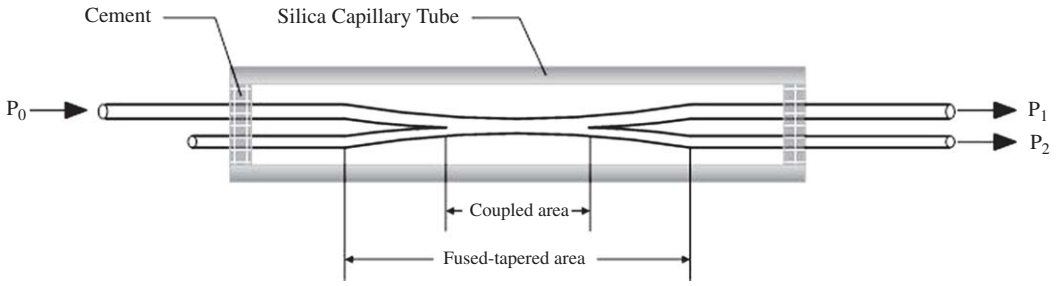


**Fig. 1.** Schematic illustration of FOAES.

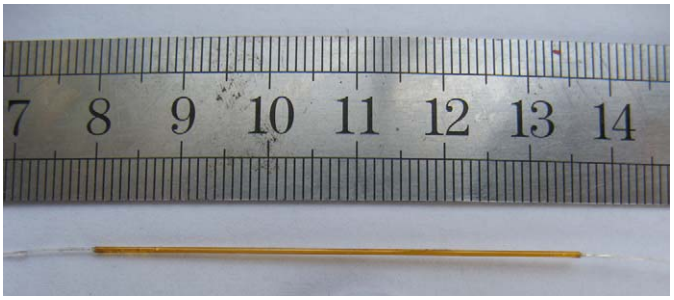


**Fig. 2.** Picture of FOAES.

and 2. The acoustic emission (AE) sensor was manufactured by placing two single-mode optical fibers in intimate parallel contact and then stretching them under a hydrogen flame. The resultant structure of the coupler consisted of a thin coupled area and fused-tapered area. The coupler is packed with silica capillary tube to protect it straight, not broken and not polluted. The silica capillary tube was about 55 mm in length, 0.7 mm in external diameter and 0.5 mm in inner diameter. Both the capillary tube and the fused-tapered fiber coupler are bonded with cement.

The output optical powers from the coupler are expressed as [15]:

$$P_1(l) = P_0 \cos^2\left\{\int_0^l C(z)dz\right\}, \quad (1)$$

$$P_2(l) = P_0 \sin^2\left\{\int_0^l C(z)dz\right\}, \quad (2)$$

where $P_1$, $P_2$ are the output optical powers, and $P_0$ is input optical power, respectively. $C(z)$ is the coupling coefficient along the coupling region ($z$-axis) and $l$ is the length of the coupling region.

When an external acoustic field is incident on the coupler, an internal acoustic wave is excited at the cement-bonded end of the coupler and it propagates along the coupling region. The propagation of this acoustic wave in the sensor results in the perturbation of the strain field along the coupling region. The tapered regions in the coupler act as strain concentrators and the effect of the incident acoustic wave is magnified in this region.

Therefore, the power of the outputs from the coupler can be expressed as

$$\Delta P(l) = P_1(l) - P_2(l) = P_0 \cos\left\{2\int_0^l C(z)dz\right\}. \quad (3)$$

That is, the changes output optical power provide a detailed statement about the acoustic disturbance, which describes the characteristics of acoustic emission sources.

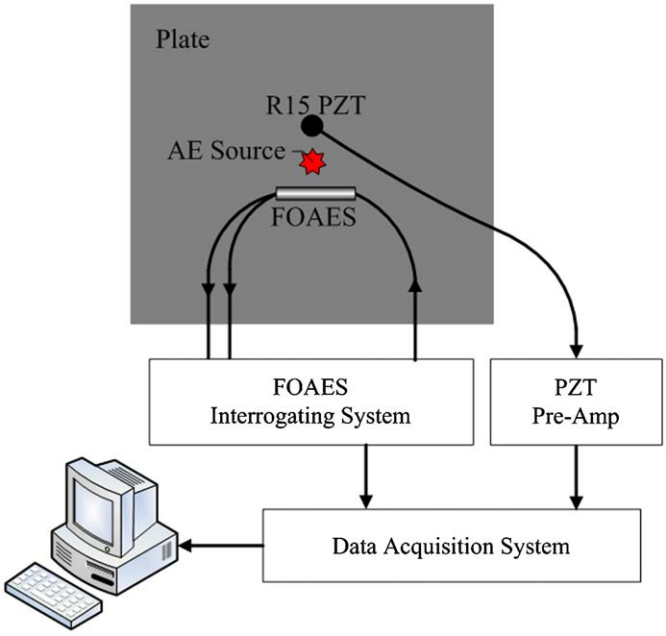


**Fig. 3.** Schematic illustration of the calibration experiment of AE sensors.

### 2.2. Calibration tests

#### 2.2.1. Experimental set-up

To validate the sensitivity of the FOAES, calibration experiments of the FOAES and the commercial piezoelectric AE sensor were carried out. Fig. 3 shows the schematic illustration of the calibration experiment of AE sensors. The fiber optic acoustic emission sensor interrogating system (FOAES interrogating system) consists of an illuminating module with a red LED, as a light source (peak wavelength 650 nm) and the detection unit consisting of two photodiodes, which is sensitive to optical radiation. The data acquisition system is PCI-2 AE System, and the piezoelectric AE sensor is R15 PZT, which are both purchased from Physical Acoustics Corporation (PAC). The software in PC always acquires and analyses the date from PCI-2 AE System. Channel One of PCI-2 AE System was connected to FOAES interrogating system, and Amp. The experimental set-up was adapted for the following experiments including comparative experiments and three-point-bending tests.

#### 2.2.2. Calibration test of specimen surface-mounted with sensors

In this paper, pencil lead break tests were adopted as calibration tests. The piezoelectric and fiber optic acoustic emission sensors were mounted on the surface of the unidirectional carbon fiber reinforced composites plate $[0^\circ_{10}]$ using coupling grease. The composite laminates (270 mm × 270

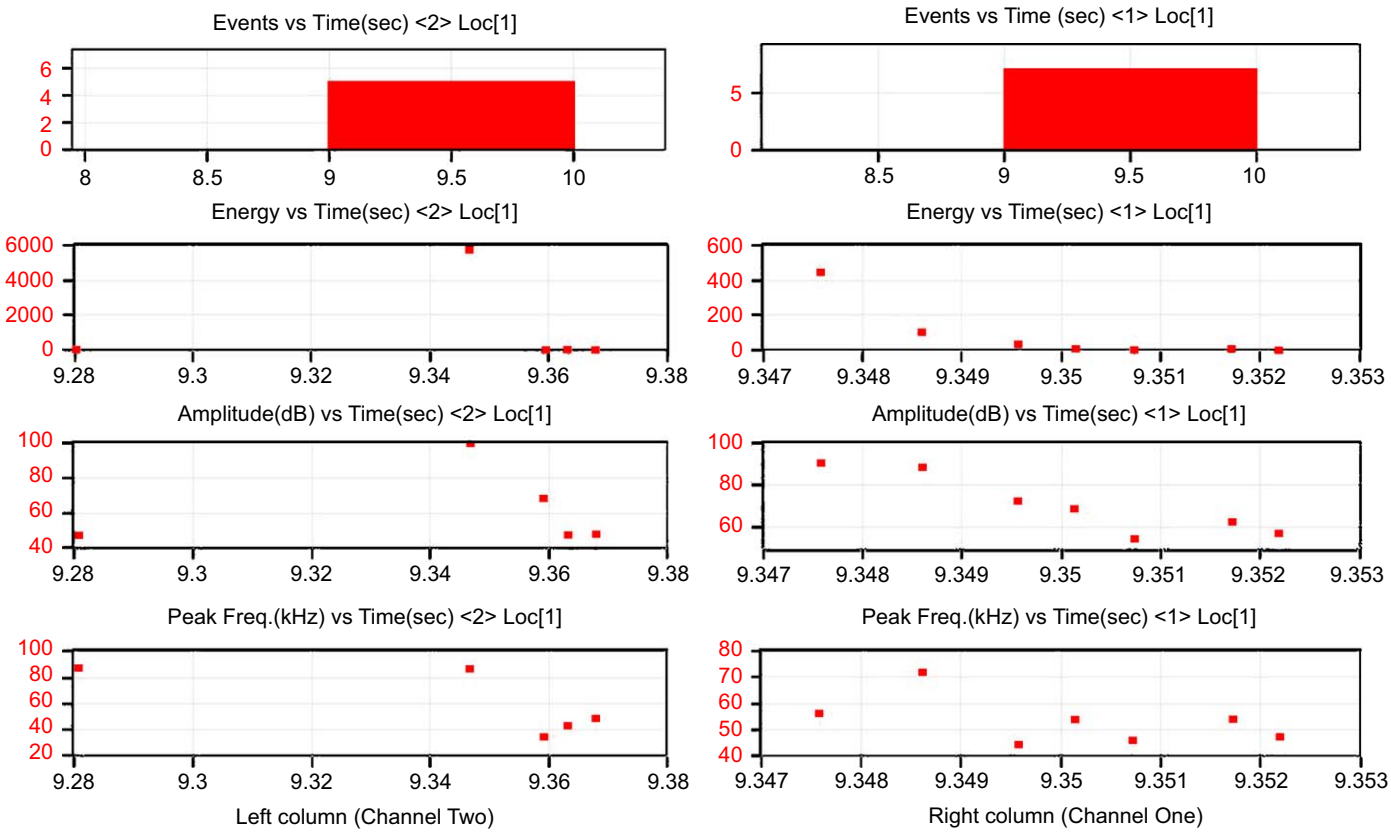


**Fig. 4.** The monitoring results from AE sensors mounted on the composite laminates.

mm × 1.5 mm) were suspended at both ends. The AE source was generated by breaking a pencil lead (φ = 0.5 mm, 2H) at point AE on the composite plate. The pencil lead break was initiated 10 mm from the piezoelectric and fiber optic acoustic emission sensors.

The results of the calibration experiment of AE sensors were shown in Fig. 4, where the left column (Channel Two) was from R15 PZT and the right column (Channel One) was from FOAES. In every column, there are four graphs including "Events", "Energy", "Amplitude" and "Peak Frequency". The four characteristic parameters are able to describe the acoustic emission basically. Every point in graphs represents a typical waveform of acoustic emission event. Scalar quantity is adopted to scale the quantities of acoustic emission "energy" from experiments.

In Fig. 4, when the pencil broke at time T = 9 s, both sensors monitored the AE signals. When the pencil lead breaks every time, it generates acoustic emission with different energy. The fiber optic sensor detected seven events, and the largest energy event was more than 400. R15 PZT detected five events, and the largest energy event was close to 6000. Because two sensors were pre-amplified differently, AE events detected by different sensors were obviously different in energy. However, it is reasonable that AE events detected by the same sensor were compared in different tests. AE events in FOAES "Amplitude" graph were similar to those in R15 PZT "Amplitude" graph. AE events in both "Peak Frequency" graphs were also similar, which is between 20 and 100 kHz.

### 2.3. *FOAES embedded in composite laminates and its calibration test*

As the fiber optic sensor has a small size and is flexible, it is easy to be embedded into composite structure. In this test, FOAES was embedded into the middle layer of the unidirectional composite laminates $[0^{\circ}_{14}]$. The composite laminates were produced from epoxy/carbon fiber prepregs. The FOAES was embedded in the middle layer of composite structures, and the embedded composite structures were heated at 170 °C in a press heater for about 7 h. The dimension of the molded composite structures was 200 mm × 17 mm × 2 mm.

Embedded FOAES in the composite structures was able to monitor damages of the whole composite laminates. R15 PZT was surface-mounted on the composite structures to monitor acoustic emission signal activated by pencil lead break in calibration experiments.

In Fig. 5, FOAES embedded in composite laminates detected three events, and the largest energy event was not more than 300. R15 PZT detected 7 events, and the largest energy event was close to 8000. AE events in FOAES "Amplitude" graph were similar to those in R15 PZT "Amplitude" graph. AE events in both "Peak Frequency" graphs were also similar. All three AE events in FOAES "Peak Frequency" graph fastened on the frequency of 60 kHz. All AE events in R15 PZT "Peak Frequency" graph distributed between the frequency of 40 and 60 kHz.

According to the AE events detected by R15 PZT in two different pencil lead break tests, the largest energy AE event in the first test (about 6000) was smaller than that in the second test (about 8000). That indicated that the energy released in the first test was not more than that in the second. However, the largest energy AE event detected by surface-mounted FOAES (about 400) was not smaller than that detected by embedded FOAES (about 250). The reason is attributed to the elastic waves, which were generated by pencil lead break, mainly propagated on the surface of CFRP specimen. It is advantageous to monitor the damage in composite structures using embedded FOAES. Therefore, a series of CFRP material failure tests for SHM has been carried out.

## 3. Three-point-bending test of CFRP using FOAES

In this paper, FOAES was applied in SHM of CFRP laminates during three-point-bending test. Two types of three-point-bending

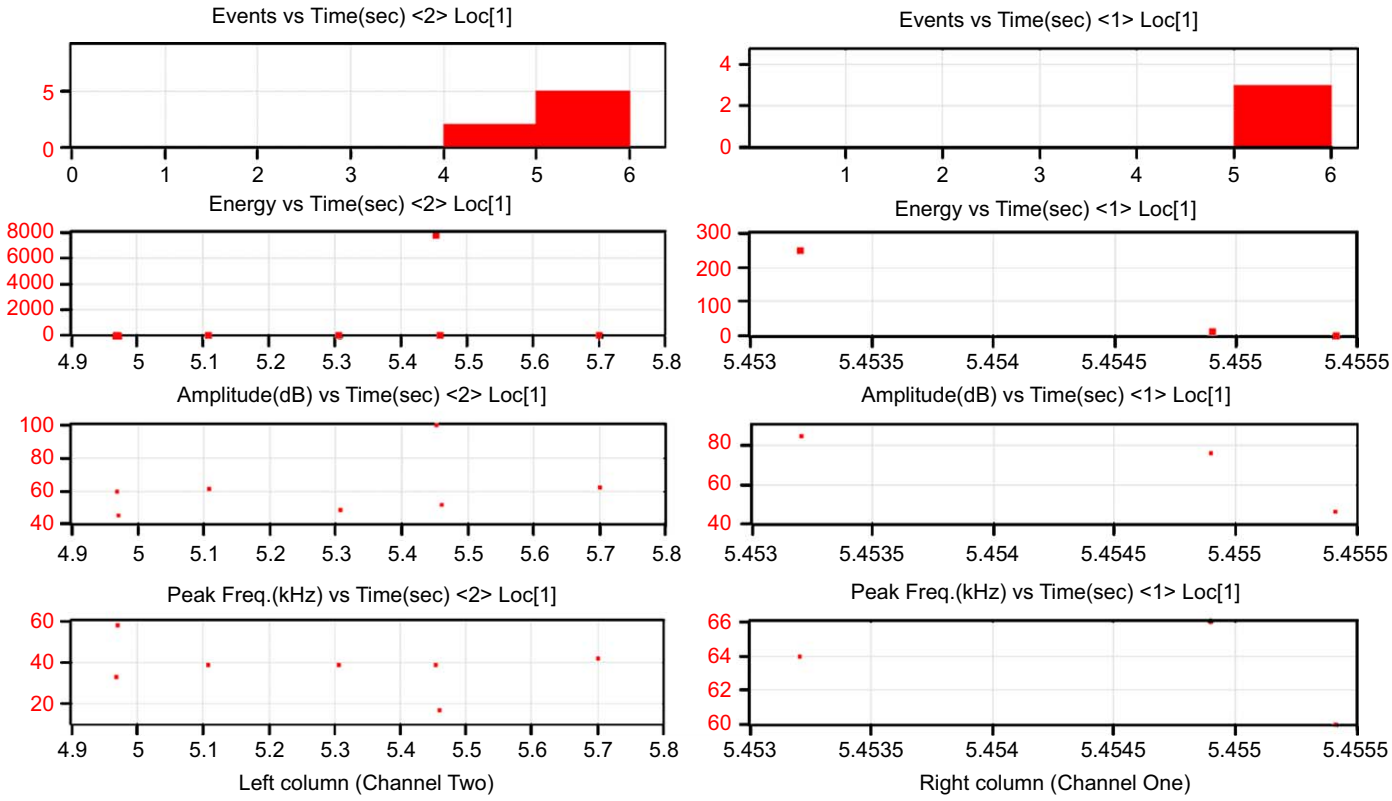


**Fig. 5.** The monitoring results from R15 PZT and composite structures embedded with FOAES.

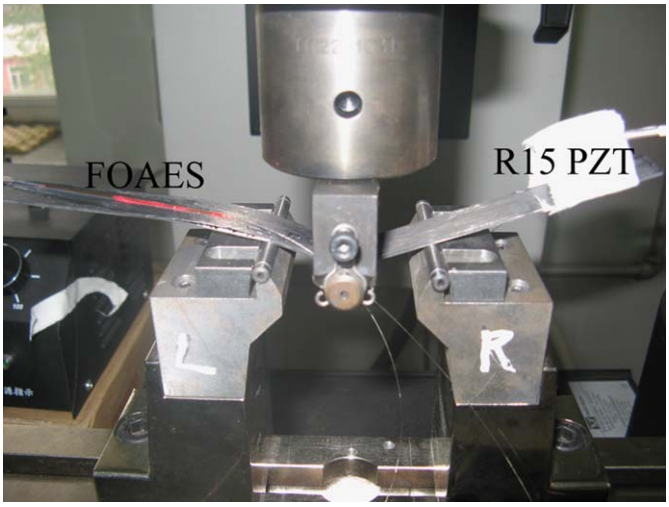


**Fig. 6.** Picture of composite laminates monitored with both sensors in three-point-bending test.

tests of composite laminates were monitored by FOAES: one test of the CFRP laminates surface-mounted with FOAES and the other test of the CFRP laminates embedded with FOAES. Bending loading was applied to the specimen using a universal test machine (INSTRON 5569).

### 3.1. Sensors surface-mounted on specimen during three-point-bending test

In this test, FOAES and R15 PZT were adopted for monitoring the damage of composite laminates on-line. Carbon fiber/epoxy composite laminates $[0^{\circ}_{10}]$ were prepared firstly, and cut into

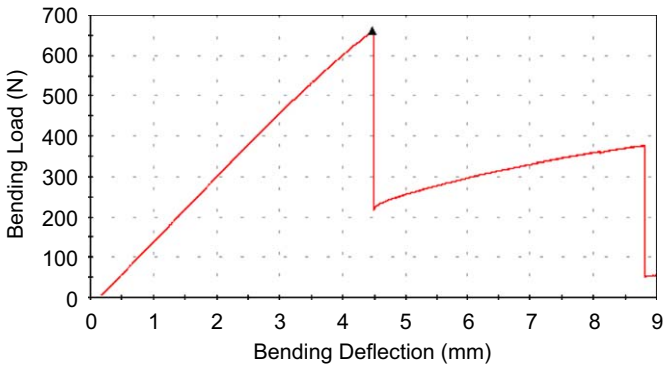


**Fig. 7.** Three-point-bending load–deflection curve.

specimens with the dimension of 200 mm × 15 mm × 1.5 mm. Both sensors were mounted on the surface of the specimen with coupling grease as shown in Fig. 6. The on-line AE acquisition system was same as shown in Fig. 3. The Loading velocity is 3 mm/min, and the span is $l = 48$ mm.

Throughout the experimental process, we constantly observe the status of samples and the results recorded from the universal test machine software and AE system software. At time $T = 272$ s, we observed the specimen state with naked eye, and saw that layers in the specimen separated. Corresponding to the load–displacement curve recorded by the software of universal test machine in Fig. 7, the load dropped down suddenly at the bending displacement of 4.49 mm, which indicated the specimen damaged. At the moment, P15 PZT and FOAES both detected strong acoustic emission energy as Fig. 8 shown. In the left column graphs, R15 PZT detected many low energy noises signals before 272 s. At time $T = 272$ s, AE event with large energy emerged. In "Energy" graph, the energy of one AE event reached

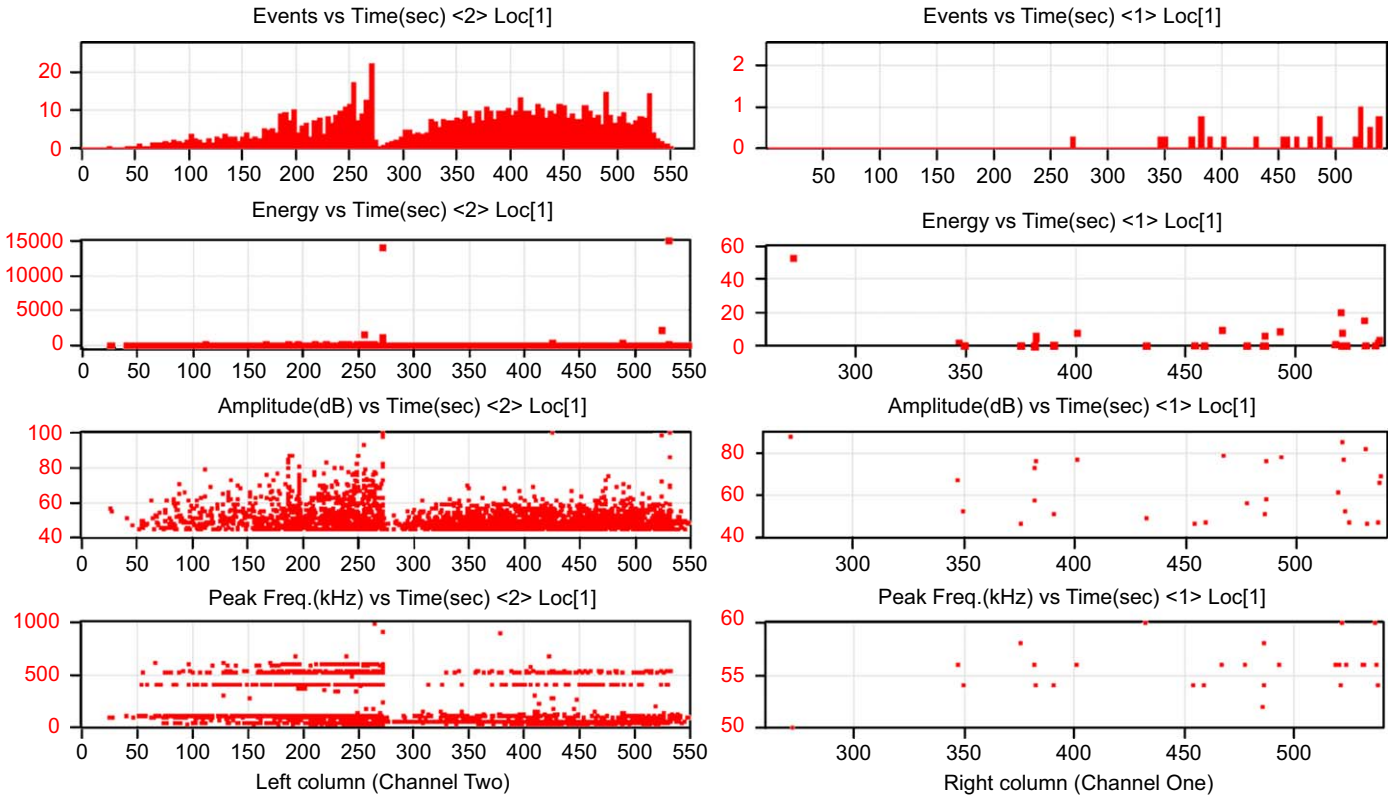


**Fig. 8.** The monitoring results from AE sensors mounted on the composite laminates.

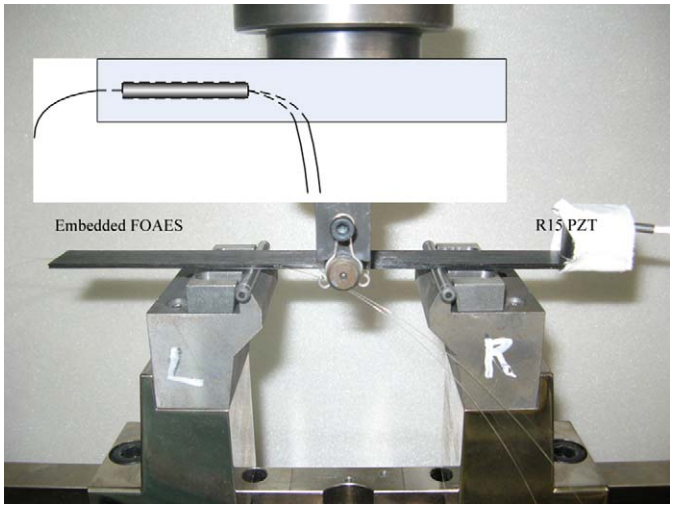


**Fig. 9.** Picture of composite laminates with embedded FOAES during test.

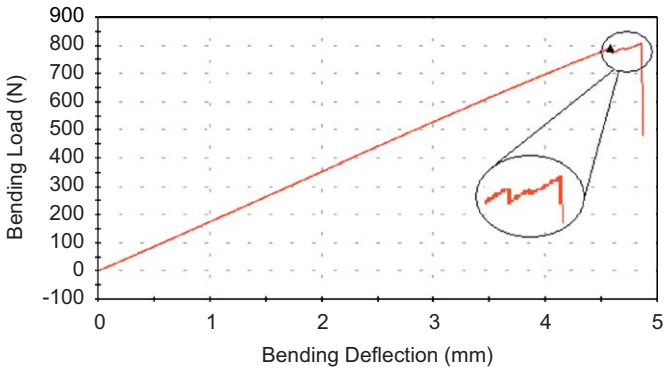


**Fig. 10.** Three-point-bending load–deflection curve.

about 15 000. In the right column graphs, At time $T = 272$ s, FOAES detected the first AE event, which was about 47 in energy in "Energy" graph. At time $T = 525$ s, we found the specimen damaged with interlaminar delamination again. In Fig. 7, the load dropped down suddenly at the bending displacement of 8.81 mm, which indicated the specimen failed. According to the results monitored with AE sensors in Fig. 8, at time $T = 525$ s, there were a large number of acoustic emission events in both "Event" graphs, and in the two "energy" images, there were a relatively high energy of the acoustic emission event, respectively.

The test proved that when the specimen failed, load–displacement curve fluctuated, and AE monitoring system detected AE signal. According with the time of AE signal appearing, we could judge the time of the specimen damage.

### 3.2. FOAES embedded in composite laminates and its test

Firstly, composite laminates embedded with FOAES were fabricated. FOAES was embedded into the middle layer of the unidirectional composite laminates $[0^\circ_{14}]$, and R15 PZT was mounted on the specimen shown in Fig. 9. The dimension of the molded composite structures was 200 mm × 17 mm × 2 mm. The set-up on-line for AE acquisition system was same as shown in Fig. 2. The loading velocity is 2 mm/min, and the span is 64 mm.

Throughout the experimental process, we constantly observe the status of samples and the results recorded from the universal test machine software and AE system software. We found that layers in the specimen separated at time $T = 140$, 147 and 148 s,

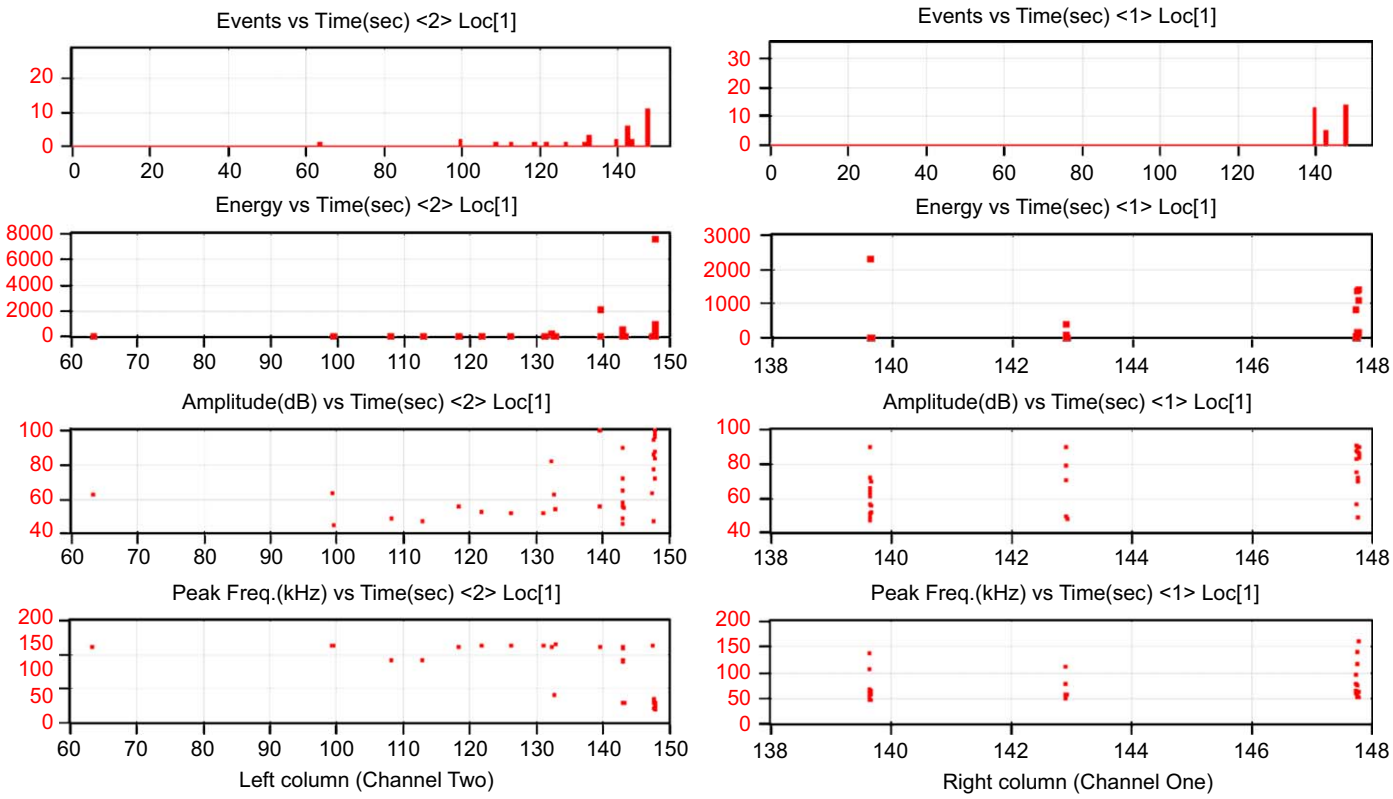


**Fig. 11.** The monitoring results from AE sensors.

respectively. According to the zoom-in part of load–displacement curve in Fig. 10, there are three fluctuations on the curve at the bending displacement of 4.59, 4.70 and 4.86 mm. According to the results detected with sensors shown in Fig. 11, we can clearly see that acoustic emission events concentrated in the three time, each time acoustic emission events concentrated in matched the fluctuations of the load-displacement curve in Fig. 10.

According to the zoom-in part of load–displacement curve in Fig. 10, at about time $T = 140$ s, the load fell, and we observed the serious damage of specimen. At the moment, according to Fig. 10, the FOAES detected more than ten AE events. At about time $T = 143$ s, there was a small fluctuation on the load-displacement curve, which indicated the specimen emerged slight damage. And the FOAES detected several AE events. At about time $T = 148$ s, the load–displacement curve fell rapidly, the specimen failed, and the FOAES detected more AE events. Large energy of elastic wave released with serious damage of specimen, and a lot of AE events emerged; Little energy of elastic wave released with slight damage of specimen, and only several AE events emerged. The test results proved that the quantity of the elastic wave energy depended on the degree of specimen damage. In order to determine the extent of specimen damage, acoustic emission sensors could detect the quantity of the elastic wave energy and the number of acoustic emission events.

## 4. Conclusions

An embedded FOAES was proposed and demarcated in pencil lead break tests in this paper. The calibration tests proved that this FOAES was able to monitor damages of composite laminates on-line as the commercial piezoelectric acoustic emission sensor did. Both the surface-mounted and the embedded monitoring methods were compared to monitoring CFRP laminates damages in its application for SHM during three-point-bending tests. The results proved that FOAES could detect elastic wave released from the specimen damage to determine the specimen damage time, and also could detect the elastic wave energy to determine the extent of specimen damage. Furthermore, the fiber optic acoustic emission sensor (FOAES) has potential advantages for structural health monitoring (SHM) of commercial composite structures in the near future, such as aerospace, wind turbine, automotive and etc.

## References

[1] Leng J, Asundi A. Non-destructive evaluation of smart materials by using extrinsic Fabry-Perot interferometric and fiber Bragg grating sensors. NDT&E Int 2002;35:273–6.
[2] Leng J, Asundi A. Structural health monitoring of smart composite materials by using EFPI and FBG sensors. Sensors and Actuators A 2003;103:330–40.
[3] Leng J, Asundi A. Real-time cure monitoring of smart composite materials using extrinsic Fabry-Perot Interferometer and fibre Bragg grating sensors. Smart materials and structures 2002;11:249–55.
[4] Leng J, Asundi A. NDE of smart structures using multimode fiber optic vibration sensor. NDT&E Int 2002;35:45–51.
[5] Gong J, MacAlpine JMK, Jin W, Liao Y. Locating acoustic emission with an amplitude-multiplexed acoustic sensor array based on a modified Mach–Zehnder interferometer. Applied Optics 2001;40:6199–202.
[6] Kim D, Koo B, Kim C, Hong C. Damage detection of composite structures using a stabilized extrinsic Fabry–Perot interferometric sensor system. Smart Materials and Structures 2004;13:593–8.
[7] Borinski JW, Boyd CD, Dietz JA. Fiber optic sensors for predictive health monitoring. AUTOTESTCON Proceedings/2001: Valley Forge, PA: IEEE Systems Readiness Technology Conference 2001, p. 250–62.
[8] Yuan L, Zhou L, Jin W. Detection of acoustic emission in structure using Sagnac-like fiber-loop interometer. Sensors and Actuators A 2005;118(1):6–13.
[9] Tandon N, Mata S. Detection of defects in gears by acoustic emission measurements. Acoustic Emission 1999;17(1–2):23–7.
[10] Lee J, Tsuda H, Toyama N. Impact wave and damage detections using a strain-free fiber Bragg grating ultrasonic receiver. NDT & E International 2007;40:85–93.

[11] Chen R, Fernando GF, Bradshaw T, Badcock RA. A novel ultrasound fibre optic sensor based on a fused-tapered optical fibre coupler. Measurement Science and Technology 2004;15:1490–5.
[12] Chen R, Bradshaw T, Burns J, Cole P, Jarman P, Pedder D, et al. Linear location of acoustic emission using a pair of novel fibre optic sensors. Measurement Science and Technology 2006;17:2313–8.
[13] Hao J, Leng J, Zhang. Non-destructive evaluation of composite pressure vessel by using FBG sensors. Chinese Journal of Aeronautics 2007;20:120–3.
[14] Fu T, Fan J, Wang C, Liu T, Leng J. A novel multifunctional optical fiber sensor based on FBG and fiber optic coupler. In: Proceedings of SPIE, vol. 6933. SPIE.
[15] Zhang J, et al. Measurements and analyses of the fields in fused tapered single-mode fiber couplers. Applied Optics 1989;28:2026–30.